

## **Siglec-9 regulates an effector memory CD8<sup>+</sup> T-cell subset that congregates in the melanoma tumor microenvironment**

**Short title:** Characterization of Siglec-9<sup>+</sup> CD8<sup>+</sup> T cells

**Author list:** Quentin Haas<sup>1</sup>, Kayluz Frias Boligan<sup>1</sup>, Camilla Jandus<sup>1,2</sup>, Christoph Schneider<sup>1</sup>, Cedric Simillion<sup>3</sup>, Michal A. Stanczak<sup>4,5</sup>, Monika Haubitz<sup>6</sup>, Seyed Morteza Seyed Jafari<sup>7</sup>, Alfred Zippelius<sup>4,5</sup>, Gabriela M. Baerlocher<sup>6,8</sup>, Heinz Läubli<sup>4,5</sup>, Robert E. Hunger<sup>7</sup>, Pedro Romero<sup>2</sup>, Hans-Uwe Simon<sup>1</sup>, Stephan von Gunten<sup>1</sup>

<sup>1</sup> Institute of Pharmacology, University of Bern, Bern, Switzerland.

<sup>2</sup> Department of Oncology UNIL CHUV, University of Lausanne, Lausanne, Switzerland.

<sup>3</sup> Department for BioMedical Research (DBMR), University of Bern, Bern, Switzerland.

<sup>4</sup> Cancer Immunology Laboratory, Department of Biomedicine, University Hospital Basel, Switzerland.

<sup>5</sup> Division of Oncology, Department of Internal Medicine, University Hospital Basel, Switzerland

<sup>6</sup> Experimental Hematology, Department of BioMedical Research, University of Bern, Bern, Switzerland.

<sup>7</sup> Department of Dermatology, Inselspital, Bern University Hospital, Bern, University of Bern, Switzerland.

<sup>8</sup> Department of Hematology, University Hospital of Bern, Bern, Switzerland.

**\*Corresponding author:** Stephan von Gunten, Institute of Pharmacology, University of Bern, Inselspital INO-F, CH-3010 Bern, Switzerland. Tel.: +41 31 632 32 98; Fax: +41 31 632 49 94. E-mail: stephan.vongunten@pki.unibe.ch

## ABSTRACT

Emerging evidence suggests an immunosuppressive role of altered tumor glycosylation due to downregulation of innate immune responses via immunoregulatory Siglecs. In contrast, human T cells, a major anti-cancer effector cell, only rarely express Siglecs. However, here, we report that the majority of intratumoral, but not peripheral blood, cytotoxic CD8<sup>+</sup> T cells expressed Siglec-9 in melanoma. We identified Siglec-9<sup>+</sup> CD8<sup>+</sup> T cells as a subset of effector memory cells with high functional capacity and signatures of clonal expansion. This cytotoxic T-cell subset was functionally inhibited in the presence of Siglec-9 ligands or by Siglec-9 engagement by specific antibodies. TCR signaling pathways and key effector functions (cytotoxicity, cytokine production) of CD8<sup>+</sup> T cells were suppressed by Siglec-9 engagement, which was associated with the phosphorylation of the inhibitory protein tyrosine phosphatase SHP-1, but not SHP-2. Expression of cognate Siglec-9 ligands was observed on the majority of tumor cells in primary and metastatic melanoma specimens. Targeting the tumor-restricted, glycosylation-dependent Siglec-9 axis may unleash this intratumoral T-cell subset, while confining T-cell activation to the tumor microenvironment.

## INTRODUCTION

Breakthroughs in T cell-based immunotherapeutic strategies have led to unprecedented and long-lasting clinical responses in a growing number of patients with advanced-stage melanoma and in an increasing number of other cancers (1,2). Clinical responses have been achieved by immune checkpoint therapies targeting inhibitory receptors on CD8<sup>+</sup> T cells in order to exploit their antitumor effector functions (1–4). These results also highlight the importance of cytotoxic CD8<sup>+</sup> T cells and the need to understand the mechanisms that restrain this population (5–8).

Altered tumor cell surface glycosylation is common and has been extensively exploited for diagnostic purposes (9), such as the detection of cancer antigen (CA) 15-3, CA 19-9, and CA 125, yet, evidence also suggests a role for glycosylation in cancer immunity (10,11). A frequent feature in cancer is hypersialylation, the overexpression of sialic acids, which are considered markers of ‘self’ and have been referred to as self-associated molecular patterns (SAMPs) (10,12). By recognizing specific sialic acid-containing glycans (sialoglycans), inhibitory CD33-related Siglecs, which contain at least one classical immunoreceptor tyrosine-based inhibition motif (ITIM) (13,14), downregulate antitumor responses of innate immune cells, including NK cells, macrophages, or neutrophils (15–18). Siglecs specifically recognize certain sialoglycans based on their chemical structure, yet, the identity and the tissue expression of Siglec ligands remain to be explored. However, evidence from lectin staining assays (16,19) or from biosynthetic pathway expression analysis based on data from The Cancer Genome Atlas (TCGA) (20) suggests overexpression of distinct Siglec ligands in different types of cancer. The tumor-associated antigen MUC1 has been identified as a ligand of Siglec-9 (18).

In contrast to other hominids, only a minority of circulating human T cells express Siglec-9 (21,22), and structural differences of CD33-related Siglecs,

involving gene deletion, gene conversion, or changes in binding specificity, have been linked to evolutionary changes in the sialome (23). Here, we demonstrated that the majority of tumor-infiltrating CD8<sup>+</sup> T cells in melanoma specimens expressed Siglec-9. These Siglec-9-expressing tumor-infiltrating lymphocytes (TILs), as well as circulating Siglec-9<sup>+</sup> CD8<sup>+</sup> T cells from melanoma patients and healthy donors, exhibited an effector memory phenotype. Despite the co-expression of inhibitory receptors, including PD-1, Siglec-9<sup>+</sup> CD8<sup>+</sup> T cells exhibited high proliferative and functional capabilities upon polyclonal activation *in vitro*. However, engagement by Siglec-9-specific antibodies or Siglec-9 ligands on target cells resulted in suppressed TCR signaling and effector functions, indicating the regulatory capacity of Siglec-9. Agonistic stimulation of Siglec-9 was associated with phosphorylation of the inhibitory phosphatase SHP-1, but not SHP-2, in human primary CD8<sup>+</sup> T cells. We observed that the majority of melanoma cells in both primary and metastatic lesions expressed cognate sialoglycan ligands of Siglec-9. Thus, Siglec-9 receptor-ligand interactions may result in a tumor glycosylation-dependent inhibitory circuit that functions to suppress T-cell effector responses in the tumor microenvironment.

## METHODS

### *Cells and tissues*

Blood from healthy donors (n=60) and melanoma patients (n=8) was collected upon written informed consent or buffy coats were purchased from the Blood Transfusion Center of Bern, Switzerland. All donors were older than 18 years old. Donors with a history of blood or immunological disorder, or donors receiving immunomodulatory drugs or chemotherapeutic interventions within 6 months before blood withdrawal were excluded. Only patients with histologically confirmed metastatic malignant melanoma were included. Peripheral blood mononuclear cells (PBMCs) were obtained by density centrifugation using Pancoll solution (PAN-Biotech, Aidenbach, Germany). For functional experiments, CD8<sup>+</sup> T-cells were isolated using the EasySep™ Human CD8<sup>+</sup> T-Cell Isolation Kit (StemCell Technologies, Vancouver, Canada), according to the manufacturer's instructions. Purity of isolated cells was always >95%. For experiments with Siglec-9<sup>+</sup> and Siglec-9<sup>-</sup> CD8<sup>+</sup> T-cell subsets, cells were isolated using fluorescence-activated cell sorting (FACS Aria, BD Biosciences, Franklin Lakes, USA) using antibody against siglec-9 (FAB1139A, R&D Systems, Minneapolis, USA). The purity of each sorted subset was >99%.

Written informed consent was obtained from all patients prior to tissue sample collection. Surgical specimens were mechanically dissociated and digested in RPMI (Sigma-Aldrich, Missouri, USA) supplemented with accutase at 1:1 dilution in medium (L11-007; PAA Laboratories, Etobicoke, Canada), collagenase IV (1 mg/mL; Worthington, Columbus, USA), hyaluronidase (1 mg/mL; MilliporeSigma, Burlington, USA), and DNase type I (10 U/mL; MilliporeSigma), filtered (Corning cell strainer, 40 µm; Sigma-Aldrich), washed in RPMI medium containing 10% fetal calf serum (FCS) (Life Technologies, Carlsbad, CA, USA) and 1% penicillin/streptomycin (Life

Technologies). Cells were frozen for future analysis in FCS containing 10% dimethyl sulfoxide (Sigma-Aldrich).

Melanoma tissue microarrays were purchased from US Biomax (Houston, USA) and contained primary melanoma, metastatic melanoma, and control tissues (intradermal nevus). All studies using human material were in accordance with the guidelines of, and approved by the cantonal ethical committees of, Bern and Basel, Switzerland. Written informed consent was received from participants prior to inclusion in the study.

### *Cell lines*

The human melanoma cell line Me275 (established at the Ludwig Cancer Institute in Lausanne Switzerland, provided by Pedro Romero) and the human acute monocytic leukemia cell line THP1 (ATCC) were cultured in RPMI medium (Sigma-Aldrich) containing 10% fetal calf serum (Life Technologies) and 1% penicillin/streptomycin (Life Technologies). Both human cell lines were used exclusively between passages 3 and 6. THP1 cell line authentication was performed by Microsynth (Balgach, Switzerland) by the short-tandem repeat method (PowerPlex16, Promega). For the redirected cytotoxic assay, the mouse mastocytoma cell line P815 (from American Type Culture Collection [ATCC], Manassas, VA, USA) was used exclusively between passage 5 and 8. This cell line was authenticated by the short-tandem repeat method but not further authenticated in the past years. The cell line was cultured in DMEM medium (Sigma-Aldrich) containing 10% fetal calf serum (FCS; Life Technologies) and 1% penicillin/streptomycin (Life Technologies), supplemented or not with murine IFN $\gamma$  (1000 U/mL; PeproTech, Rocky Hill, USA). No mycoplasma testing was performed for the cell lines.

### *Cell culture*

Isolated CD8<sup>+</sup> T cells were cultured in RPMI medium (Sigma-Aldrich) containing 10% fetal calf serum (FCS) (Life Technologies) and 1% penicillin/streptomycin (Life Technologies) supplemented with rhIL2 (100 U/mL; PeproTech). When required, cells were activated with plate-bound anti-CD3 (1 µg/mL; OKT-3, BioXcell, West Lebanon, USA) and soluble anti-CD28 (1 µg/mL, BioLegend California, USA) for 1 hour at 37°C in supplemented medium and cultured in presence or absence of IL12 (50 ng/mL), IL21 (20 ng/mL), IL5 (20 ng/mL), IL10 (40 ng/mL), IL15 (100 ng/mL), IL18 (100 ng/mL), or LPS (100 ng/mL)(all from PeproTech). .

### *Flow cytometry*

PBMCs, lymphocytes isolated from melanoma tissues, or purified CD8<sup>+</sup> T cells were labeled using fluorescent mAbs directed against surface molecules (20 minutes at 4°C), washed in PBS with 0.2% BSA (Sigma-Aldrich), and acquired using a FACSVerse (BD Biosciences). A minimum of 100,000 cells was used for each staining. When required, cells were blocked using FC-block (human TruStain FcX, Biolegend) and viability was analyzed using Zombie NIR viability kit (BioLegend). Cells were labeled either directly *ex vivo* or, where indicated, after 30 minutes of treatment with neuraminidase (25 mU; Roche Diagnostics, Rotkreuz, Switzerland) at 37°C. Intracellular cytokine staining was done at 4°C for 30 minutes.

Isolated CD8<sup>+</sup> T cells were stimulated for 1 hour at 37°C in 5% CO<sub>2</sub> with anti-CD3 (1 µg/mL, plate bound) and anti-CD28 (1 µg/mL, soluble) or with anti-CD3 mAb-coated P815 cells. Thereafter, GolgiPlug and GolgiStop (BD Biosciences) were added to the cultures followed by incubation for 5 hours. Cells were spun down and incubated with fluorochrome-conjugated mAbs against surface markers. Cells were then washed, fixed with 2% paraformaldehyde in PBS, permeabilized in PBS

supplemented with 2% heat-inactivated FCS, 2mM EDTA, and 0.5% saponin (all from Sigma-Aldrich), and stained intracellularly with fluorochrome-conjugated mAbs against cytokines TNF $\alpha$  (MAB11, eBioscience, Waltham, USA) and IFN $\gamma$  (4S.B3, BioLegend) or ZAP-70 (PY292, J34-602, BDBiosciences) and SLP-76 (PY128, J141-668.36.58, BDBiosciences). Finally, cells were washed in PBS and analyzed on a BD FACSVerse (BD Biosciences). Data were analyzed with FlowJo 10.0.6 software (Tree Star Inc, Oregon, USA).

For surface staining, fluorochrome-conjugated antibodies against CCR3 (5.E.8), CCR5 (HEK/1/85a), CXCR6 (TG3/CXCR6), CCR9 (L053E8), Integrin  $\alpha_4\beta_7$  (FIB27), BTLA (MIH26), PD-1 (EH12.1), CTLA-4 (BNI3), Tim-3 (7D3), mouse PD-L1 (MIH5), and mouse PD-L2 (TY25) were purchased from BioLegend. The fluorochrome-conjugated antibodies against CD3 (SK7), CD8 (RPA-T8), CLA (HECA-452), TCR $\alpha\beta$  (IP26), CD45RA (HI100), LAG3 (T47-530), CXCR3 (1C6/CXCR3), CCR4 (1G1), CD107a (H4A3), ZAP-70 (PY292, J34-602), SLP-76 (PY128, J141-668.36.58), and CCR7 (G043H7) were purchased from BD Biosciences, whereas Siglec-9 (191240), CCR1 (53504), and CCR7 (150503) were from R&D Systems). Each mAb was titrated on PBMCs before use. Data analysis was performed using FlowJo (V10.4.2, Tree Star Inc.).

### *Immunostaining of tissue sections*

Detection of Siglec-9 ligands by immunofluorescence was performed as previously described (16). Paraffin-embedded tissue sections from melanoma or tissue microarrays (TMA) were deparaffinised with NeoClear (MilliporeSigma) and graded ethanol (ranging from 100% to 40%). Antigen retrieval was performed by heating the sections in 0.1M citrate buffer (Dako, Santa Clara, USA) pH 6.0 three times for 3 minutes in a microwave, with intermediate cooling 8 incubations of 20 minutes. For

the Siglec-9 ligands staining, recombinant human Siglec-9 hFc (10  $\mu$ g/mL; R&D Systems) was pre-incubated with PE-conjugated goat anti-human Ig (polyclonal, Jackson ImmunoResearch Laboratories, West Grove, USA) diluted 1/100 in PBS containing 10% fetal calf serum (Life Technologies) and 1% penicillin/streptomycin (Life Technologies) for 1 hour at 4°C and then applied to the tissue samples for 1 hour at room temperature. For the selection of specific tumor areas, the tissue samples were co-stained with the melanoma marker 13 melan-A (Dako). Sections were incubated with 4',6-Diamidin-2-phenylindol (DAPI, Thermo Fischer Scientific, Waltham, USA) for nuclei detection and mounted in ProLong<sup>TM</sup> Gold Antifade Reagent (Invitrogen, Darmstadt, Germany). Stained samples were scanned using a Panoramic MIDI slide scanner (Histech 3D, Budapest, Hungary) or by confocal microscopy (LSM 700; Carl Zeiss, Oberkochen, Germany). Acquired images were analyzed using 17 the ImageJ software version 1.51 (NIH, Bethesda, USA) or QuPath(24).

#### *Telomere length measurement by automated multicolor flow-FISH 20*

For telomere length analysis, human CD8<sup>+</sup> T cell Siglec-9<sup>+</sup> and Siglec-9<sup>-</sup> subsets were isolated from the peripheral blood of 3 healthy donors by fluorescence-activated cell sorting as described above. Telomere length measurement by *in situ* hybridization and flow cytometry (automated multicolor flow-FISH) was then performed as previously described(16).  $2.5 \times 10^3$  to  $2 \times 10^6$  cells were used for *in situ* hybridization. Cells were incubated with 170  $\mu$ L hybridization mixture containing 75% deionized formamide (Sigma-Aldrich), 20 mM Tris (pH 7.1; Sigma-Aldrich), and 1% BSA (Sigma-Aldrich) with no probe (unstained) or with telomere-specific FITC conjugated (C<sub>3</sub>TA<sub>2</sub>)<sub>3</sub> peptide nucleic acid (PNA) (0.3  $\mu$ g/mL; Applied Biosystems, Foster City, USA). Denaturation was done at 87°C for 15 minutes, and hybridization

was performed in the dark and at room temperature for 90 minutes. Excess and non-specifically bound telomere PNA probe was removed by 4 washing steps at room temperature using 1 ml washing solution containing 75% formamide, 10 mM Tris, 0.1% BSA, and 0.1% Tween 20 (Sigma-Aldrich), followed by washing with 1mL solution containing PBS, 0.1% BSA, and 0.1% Tween 20 at room temperature. DNA counterstaining was performed using a solution containing Sheath Fluid (BD Bioscience), 0.1% BSA, and a sub-saturating amount of LDS 751 (0.01 36  $\mu$ g/mL; Invitrogen) overnight. Acquisition of telomere fluorescence was performed using FACS Calibur (BD Biosciences). For each sample, unstained and telomere stained samples were tested. FlowJo version 10 (Tree Star Inc.) was used for analysis of telomere length in the specific cell subsets. Specific telomere fluorescence was determined as the difference between the fluorescence of the stained samples minus the (auto-) fluorescence of the corresponding unstained sample. Using calibration beads and an internal standard of cow thymocytes, the telomere fluorescence was calculated into kilobases of telomere length.

### *Immunoblotting*

For immunoblotting analysis antibodies against phosphorylated SHP-1 (polyclonal) and total SHP-1 (clone Y476) were both purchased from Abcam (Cambridge, UK) and diluted 1/1000 in PBS supplemented with 0.05% Tween (Sigma-Aldrich) and 5% BSA. Antibodies against phosphorylated SHP-2 (polyclonal) and total SHP-2 (clone D50F2) were purchased from Cell Signaling Technologies (Massachusetts, USA) and diluted 1/1000 in PBS supplemented with 0.05% Tween (Sigma-Aldrich) and 5% BSA. Siglec-9 agonistic antibody (E10-286) was provided by BD Pharmingen (San Diego, USA) and used at an optimized concentration of 3 $\mu$ g/mL. Capturing Siglec-9 antibodies were provided by R&D Systems. For detection of SHP-1 and SHP-2

phosphorylation, CD8<sup>+</sup> T cells were stimulated with agonistic anti-siglec-9 (E10-286) or isotype control (3 µg/mL, mouse IgG1, clone MG1-45, BD Biosciences) for different time points. Thereafter, the cells were harvested, washed, and lysed on ice for 30 min in RIPA buffer with protease inhibitor (P8340) and phosphatase inhibitor (P5726) cocktails (all from Sigma-Aldrich) diluted 1/100. The cell lysates were cleared by centrifugation at 14,000 rpm for 15 minutes. Protein content of samples was assessed Pierce BCA protein assay kit (Thermo Fisher Scientific), and 20 µg of total proteins per well were used for the assay. Lysates were boiled for 5 minutes, proteins were separated by SDS-PAGE, and transferred to PVDF membranes. Membranes were blocked with 5% BSA (Sigma-Aldrich) and probed overnight with antibodies against total or phosphorylated SHP-1 or pSHP-2. In all cases, the signal was detected using an anti-rabbit-HRP secondary antibody (GE Healthcare, Chicago, USA) diluted 1/10,000 in PBS supplemented with 0.05% Tween (Sigma-Aldrich) and 5% BSA and revealed by the addition of Luminata Forte (Millipore) according to the manufacturer's protocol. Exposure was done using an Odyssey Infrared Imaging System (LI-COR Biosciences, Lincoln, USA).

#### *RNA analysis on TCGA database*

Data were obtained from TCGA-SKCM project (Project ID; dbGaP Study Accession: phs000178) There was no inclusion or exclusion criteria applied. The study represents 469 patients. The results shown here are based upon data generated by the TCGA Research Network: <http://cancergenome.nih.gov/>. The publicly available TCGA datasets were downloaded from the TCGA Data Portal at <https://tcga-data.nci.nih.gov/tcga/>. The detailed information of the TCGA data structures can be reviewed at <https://tcga-data.nci.nih.gov/tcga/tcgaDataType.jsp>. The detailed information of the RNA-Seq experiments, protocols, and software used can be found

at the TCGA Data Portal at <https://tcga-data.nci.nih.gov/tcga/>. Data was retrieved on Aug 21<sup>st</sup>, 2017. Values represent normalized, and log-transformed read counts (log-transformed RPKM values). Figures were created in R version 3.4.2 (Bell Laboratories, formerly AT&T, now Lucent Technologies, USA) using the heatmap2 and the ggplot2 library. Dendrogram clustering algorithm was used for Figure 2. The ranking of cliques as high, moderate, and low expression in Figure 2 is an arbitrary denomination to distinguish the cliques; no preliminary cutoff was determined.

### *Proliferation assay*

Purified human CD8<sup>+</sup> T cells were labeled with a final concentration of 5 $\mu$ M CFSE (Molecular Probes, Thermo Fisher Scientific) according to the manufacturer's instructions. Cells were activated using anti-CD3 and anti-CD28 as described above, and cultured in complete RPMI medium supplemented with rhIL2 (100U/mL, Peprotech). CFSE fluorescence was evaluated at day 4 by flow cytometry.

### *CD107a mobilization assay*

Purified human CD8<sup>+</sup> T cells were incubated at a 3:1 ratio with P815 target cells for 4 hours, in the presence of FITC-conjugated anti-CD107a (BioLegend) in a dilution of 2/100. After incubation, cells were washed with PBS plus 0.2% BSA (Sigma-Aldrich) and analyzed on a FACSVerse (BD Biosciences). Where indicated, target cells were pretreated with neuraminidase (25 mU; Roche Diagnostics) for 30 minutes at 37°C and washed extensively before coculture with CD8<sup>+</sup> T cells.

### *Redirected cytotoxicity assay*

Cytolytic CD8<sup>+</sup> T cell activity was evaluated in a redirected cytotoxicity assay against P815 cells. To this end, the P815 cells were incubated with anti-CD3 (20  $\mu$ g/mL;

OKT-3) for 1 hour. When indicated, P815 cells were treated with neuraminidase (25mU, Roche Diagnostics). CD3-coated P815 cells were cocultured (3:1 E/T ratio) with CD8<sup>+</sup> T cells pre-treated or not with monoclonal anti-PD-1 (10ug/mL, pembrolizumab, Merck & Co, USA) for 30 minutes at 37°C. After 4 hours of incubation, the specific lysis of P815 cells was assessed by measuring the LDH activity in the supernatant, with the Cytotoxicity Detection Kit<sup>PLUS</sup> LDH (Roche Diagnostics), according to the manufacturer's instructions. Specific lysis was calculated as (experimental – spontaneous release)/(total – spontaneous release)\*100 and expressed as a fold-change between treated and untreated groups (specific lysis fold-change).

#### *Enzyme-linked immunosorbent assay (ELISA)*

High-binding polystyrene microtiter plates (Thermo Fisher Scientific) were coated with anti-siglec-9 (100 µL at 10 µg/mL; R&D Systems) in coating buffer (buffer composed of 0.795 g/mL Na<sub>2</sub>CO<sub>3</sub> diluted in water, where a solution of 146.5 g/mL NaHCO<sub>3</sub> in water was added until pH reached 9,6) at 4°C overnight. Plates were washed 3 times with PBS, 5% Tween-20, and then blocked with 100 µL PBS-5% BSA for 1 hour at 37°C and washed an additional 3 times. Cell samples were lysed for 30 minutes at 4°C in NP40 Cell Lysis Buffer (Thermo Fisher Scientific) supplemented with protease inhibitor and phosphatase inhibitor cocktails (all from Sigma-Aldrich). Protein concentration of samples was determined using Pierce BCA protein assay kit (Thermo Fisher Scientific) according to manufacturer instructions. 100 µL sample lysates diluted in blocking solution to randomize concentrations were added to the wells for 2 hours at room temperature. After washing 3 times, 100 µL of anti-phospho-tyrosine-HRP (R&D Systems) diluted 5000-times in blocking buffer was added for 2 hours at room temperature. After washing 3 time, 100 µL of 3,3',5,5'-

tetramethylbenzidine (TMB; Sigma-Aldrich) was added for 10 minutes. 50  $\mu$ L of 1M HCl stop solution was added before reading on Odyssey Infrared Imaging System (LI-COR Biosciences).

### *TCRV $\beta$ sequencing*

CD8<sup>+</sup> T cells were isolated from peripheral blood of healthy donors and TILs and separated by fluorescence-activated cell sorting into Siglec-9<sup>+</sup> and Siglec-9<sup>-</sup> populations as already described. Genomic DNA from Siglec-9<sup>+</sup> and Siglec-9<sup>-</sup> subsets was extracted using NucleoSpin® Tissue kit from Macherey-Nagel (Gutenberg, France) according to the manufacturer instructions. Genomic DNA quantity and purity were assessed through spectrometric analysis. 1.47 to 29.1 ng/ $\mu$ L of genomic DNA were analyzed by high-throughput sequencing of the TCRV $\beta$  using the ImmunoSEQ immune profiling platform at the survey level (Adaptive Biotechnologies, Seattle, USA), which represents a detection capacity of 1 cell in 40,000. Raw sequence reads were demultiplexed according to Adaptive's proprietary barcode sequences. Demultiplexed reads were then further processed to remove adapter and primer sequences, identify and correct for technical errors introduced through PCR and sequencing, and remove primer dimer, germline and other contaminant sequences. The data is filtered and clustered using both the relative frequency ratio between similar clones and a modified nearest-neighbor algorithm, to merge closely related sequences. The resulting sequences were sufficient to allow annotation of the V(N)D(N)J genes constituting each unique CDR3 and the translation of the encoded CDR3 amino acid sequence. V, D and J gene definitions were based on annotation in accordance with the IMGT database ([www.imgt.org](http://www.imgt.org)). Data was analyzed using the immunoSEQ Analyzer toolset. Data are available on the following link: <https://clients.adaptivebiotech.com/pub/haas-2019-cir>.

### *Statistics*

Unless otherwise indicated, data represent mean  $\pm$  standard deviation (SD). For quantitative comparisons, Student's *t* test (2-sample 2-tailed comparison) or one-way ANOVA with Holm-Sidak's or Bonferonni post-test (multiple-sample comparison) was performed using Prism 5.0. *P* < 0.05 was considered significant.

### *Data Sharing Statement*

For original data, please contact [stephan.vongunten@pki.unibe.ch](mailto:stephan.vongunten@pki.unibe.ch).

## RESULTS

### Tumor-infiltrating effector memory CD8<sup>+</sup> T cells express Siglec-9

CD8<sup>+</sup> T cells are considered as major anti-cancer effector cells (25,26). We observed that the percentage of peripheral blood siglec-9<sup>+</sup> CD8<sup>+</sup> T cells was low in melanoma patients (n=8) and healthy individuals (n=23) (Fig. 1A-B), which is in line with previous reports of low expression of Siglecs on circulating T cells (21,22). In contrast, the majority of tumor-infiltrating CD8<sup>+</sup> T cells from melanoma patients (n=6) expressed Siglec-9, and neuraminidase treatment, which has been shown by us to unmask Siglecs on NK cells bound by sialic acid ligands *in cis* (16), had no effect on the Siglec-9 staining of healthy individual CD8<sup>+</sup> T cells (Supplementary Fig. S1). An analysis of tumors from the TCGA melanoma dataset revealed that CD8 $\alpha$  and CD8 $\beta$  (Fig. 1C), but not NKp46 expression (Supplementary Fig. S2) correlated significantly with *SIGLEC9* gene expression.

We went on to investigate phenotypic and functional characteristics of Siglec-9<sup>+</sup> CD8<sup>+</sup> T cells. Flow cytometric analysis based on CCR7 and CD45RA cell surface expression (27), revealed that the subsets of Siglec-9<sup>+</sup> CD8<sup>+</sup> T cells in the peripheral blood of healthy donors (HDs) and melanoma patients, as well as most Siglec-9<sup>+</sup> CD8<sup>+</sup> melanoma TILs, primarily exhibited an effector memory phenotype (Fig. 1D-E). Among these, the majority of Siglec-9<sup>+</sup> CD8<sup>+</sup> T cells in HD peripheral blood and patient TILs represented CCR7<sup>-</sup>CD45RA<sup>-</sup> effector memory (EM) T cells, whereas the majority of the circulating Siglec-9<sup>+</sup> CD8<sup>+</sup> T cells consisted of CCR7<sup>-</sup>CD45RA<sup>+</sup> effector memory (EMRA) T cells in melanoma patients. In tumors of the TCGA melanoma dataset, Siglec-9 mRNA expression correlated with enhanced transcription of the T-cell effector molecules granzyme B, perforin, IFN $\gamma$ , and TNF $\alpha$ .

(Fig. 1F), resembling an activation-dependent inhibitory receptor expression program as previously reported (28–30).

### **Inhibition of Siglec-9<sup>+</sup> CD8<sup>+</sup> T-cell responses by tumor cell sialoglycan ligands**

In previous work, we found expression of Siglec-9 ligands on various human melanoma cell lines and in primary tissue specimens from five melanoma patients (16). Here, we expanded this analysis to include a tissue microarray (TMA) combined with lectin immunohistochemistry using a recombinant Siglec-9–human IgG1 Fc chimera (16). We investigated Siglec-9 ligand expression in surgical resections from different patients, including primary (n=62) and metastatic melanoma (n=20) samples, as well as non-malignant intradermal naevi (IDN; n=7) specimens. In both primary and metastatic lesions, but not IDN, Siglec-9 ligands were found to be expressed, with a diffuse immunofluorescence staining pattern, on primary melanoma (mean 75.9%; range 25.0 – 97.8%) or metastatic (mean 63.4%; range 25.3 – 97.7%) melan-A<sup>+</sup> cells (Fig. 2A-C). In accordance with our previous report (16), Siglec-9 ligands were absent in normal tissue on the TMA (Fig. 2A).

The biosynthesis of specific Siglec ligands involves specific sialyltransferases (STs) that transfer sialic acids to acceptor carbohydrate residues in a linkage-dependent manner. Analysis of RNA-seq data from the TCGA database for the 20-known human STs in melanoma tumors (n=469) revealed differential expression of the ST enzymes (Fig. 2D and Supplementary Fig. S3). Among the most expressed STs were ST3GAL5, ST6GALNAC2, and ST3GAL6, which are predicted to be key enzymes involved in the biosynthesis of Siglec-9 ligands as determined by glycan array technology at the Consortium for Functional Glycomics (CFG) (<http://www.functionalglycomics.org>), and other techniques (31). Analysis of RNA-seq data from the TCGA database of melanoma tumors using a dendrogram clustering

algorithm revealed a subgroup of seven STs, including ST3GAL5, ST6GALNAC2, and ST3GAL6, with consistently high expression in most melanoma specimens (clique 4), a subgroup of six STs with moderate expression (clique 3), and seven STs with low expression (cliques 1 and 2) (Fig. 2D).

Next, we sought to examine the functional consequences of Siglec-9 engagement by its cognate ligands on T cells. P815 target cells used here express Siglec-9 ligands on their cell surface, as assessed by confocal microscopy (Fig. 2E). Enzymatic digestion using neuraminidase (sialidase) treatment was used to remove Siglec-9 sialoglycan ligands, as previously done (16). The redirected cytotoxic activity of Siglec-9<sup>+</sup> CD8<sup>+</sup> T cells from healthy donors was comparable to that of Siglec-9<sup>-</sup> cytotoxic T lymphocytes (CTLs) when cultured with anti-CD3–loaded P815 cancer cells (Fig. 2F). Enzymatic digestion of Siglec-9 surface ligands on the target cells by neuraminidase pre-treatment only enhanced the cytotoxicity of the Siglec-9<sup>+</sup> cells. Following enzymatic digestion of Siglec-9 ligands on the target cells, Siglec-9<sup>+</sup> CD8<sup>+</sup> T cells from healthy donors constitutively responded to polyclonal activation with higher degranulation (CD107a mobilization) (Fig. 2G) and intracellular cytokine production, including IFN $\gamma$  and TNF $\alpha$  (Fig. 2H-I). Expression of Siglec-9 in Jurkat cells was previously reported to result in reduced phosphorylation of ZAP-70 following TCR engagement (21). Neuraminidase treatment of target cells resulted in enhanced TCR signaling exclusively within the healthy donor Siglec-9<sup>+</sup> CD8<sup>+</sup> T-cell subset, as evidenced by ZAP-70 (Fig. 2J) and SLP-76 (Fig. 2K) phosphorylation measurement.

### **Siglec-9 triggers SHP-1–associated inhibitory pathways in CD8<sup>+</sup> T cells**

Engagement of Siglec-9 using the anti–Siglec-9 clone E10-286 has been previously shown to result in Siglec-9 phosphorylation (32) and agonistic effects on receptor

functions (16,32). In a redirected cytotoxicity assay, treatment with anti-Siglec-9 significantly reduced the killing activities of healthy donor-sorted Siglec-9<sup>+</sup>, but not Siglec-9<sup>-</sup>, CD8<sup>+</sup> T cells directed against anti-CD3–loaded P815 cells (Fig. 3A). Intracellular flow cytometric analysis revealed that treatment with E10-286 also inhibited cytokine production, including IFN $\gamma$  (Fig. 3B) and TNF $\alpha$  (Fig. 3C), exclusively in Siglec-9<sup>+</sup> CD8<sup>+</sup> T cells following co-stimulation by anti-CD3 and anti-CD28. Under these conditions, E10-286 stimulation also led to reduced phosphorylation of ZAP-70 (Fig. 3D) and SLP-76 (Fig. 3E) following TCR engagement. Given that Siglec-9 contains an immunoreceptor tyrosine-based inhibitory motif (ITIM) known to recruit tyrosine phosphatases (21,31,33), the phosphorylation of Siglec-9, as well as the activation of the SH2 domain-containing protein tyrosine phosphatases SHP1 and SHP2, in CD8<sup>+</sup> T cells was investigated. Following Siglec-9 engagement by E10-286, rapid phosphorylation of Siglec-9 (Fig. 3F) and of SHP-1 (Fig. 3G and Supplementary Fig. S4) was observed with a peak after 5 minutes. In contrast, no significant phosphorylation of SHP-2 was observed (Fig. 3G and Supplementary Fig. S4). In line with this observation, in Jurkat cells Siglec-9 has been shown to associate preferentially with SHP-1 and not SHP-2 (21). Phosphorylation of Siglec-9 appeared to occur in CD8<sup>+</sup> T cells isolated from patients TILs in comparison to unstimulated PBMCs from healthy donors (Supplementary Fig. S5). Melanoma tissue data from TCGA revealed a correlation between Siglec-9 and SHP-1, but not SHP-2 (Fig. 3H). These findings suggest a role of SHP-1–associated inhibitory pathways upon Siglec-9 engagement in CD8<sup>+</sup> T cells.

### **Functional Siglec-9<sup>+</sup> CD8<sup>+</sup> T cells derive from previous clonal expansion**

We went on to assess the functional and phenotypic characteristics of the human Siglec-9<sup>+</sup> CD8<sup>+</sup> T-cell subset. Co-stimulation with anti-CD3 and anti-CD28 resulted in

increased IFN $\gamma$  and TNF $\alpha$  production by Siglec-9<sup>+</sup> CD8<sup>+</sup> T cells isolated from healthy donors, which was more prominent compared to their Siglec-9<sup>-</sup> counterparts (Fig. 4A-B). Flow cytometric analysis of CD8<sup>+</sup> T-cell proliferation after anti-CD3 and anti-CD28 co-stimulation revealed a high proliferative capacity of the Siglec-9<sup>+</sup> CD8<sup>+</sup> T-cell subset (Fig. 4C). Together with the enhanced cytotoxicity and cytokine production observed in redirected assays (Fig. 2F-I), these data indicate that Siglec-9<sup>+</sup> CD8<sup>+</sup> T cells are functionally competent upon anti-CD3 and anti-CD28 stimulation *in vitro*.

Telomere length analysis was performed using automated multicolor flow-FISH, as previously done (16,34). The results revealed evidence for multiple rounds of prior cell division within the Siglec-9<sup>+</sup> CD8<sup>+</sup> T cells of healthy individuals, indicating past proliferative responses of these cells (Fig. 4D). This subset demonstrated a higher cell surface expression of chemokine receptors, in particular CCR5, CXCR3, and CXCR6, as determined by multiparametric flow cytometry (Fig. 4E).

To investigate the diversity of the TCR repertoire of Siglec-9<sup>+</sup> and Siglec-9<sup>-</sup> CD8<sup>+</sup> T-cell subsets from healthy peripheral blood, deep-sequencing of TCRV $\beta$  chains on genomic DNA was performed by multiplex polymerase chain reaction (PCR) assays and then sequenced using the ImmunoSEQ immune profiling platform (35). The distribution of individual clonotypes was dissimilar between the CD8<sup>+</sup> T-cell subsets, with higher frequencies of the ten top rearranged clones in the Siglec-9<sup>+</sup> CD8<sup>+</sup> T-cell subset (Fig. 4F). Despite the predominance of expanded clonotypes within the Siglec-9<sup>+</sup> CD8<sup>+</sup> T-cell subset, some nucleotide chain sequences were shared between Siglec-9<sup>+</sup> and Siglec-9<sup>-</sup> CD8<sup>+</sup> T cells, as illustrated in donor TS-02 (Fig. 4G-H), suggesting that Siglec-9 receptor expression can be acquired during the process of clonal expansion. However, polyclonal T-cell activation by CD3 and CD28 mAbs and combinations of different cytokines or tumor cell line supernatants did not induce significant Siglec-9 expression in sorted Siglec-9<sup>-</sup> cells from healthy donors

(Supplementary Fig. S6). Together, these data provide evidence of a previous clonal expansion of Siglec-9<sup>+</sup> CD8<sup>+</sup> T cells and demonstrated the high proliferative and functional capacities of this CD8<sup>+</sup> T-cell subset.

### **Analysis of tumor-infiltrating Siglec-9<sup>+</sup> CD8<sup>+</sup> T cells**

Using multiparametric flow cytometry, we examined the co-expression of Siglec-9 with known modulatory T cell receptors, including immune checkpoints CTLA-4, PD-1, BTLA, LAG3, and Tim-3 on TILs from melanoma patients (Fig. 5A). Co-expression of Siglec-9 and PD-1 was frequent, which was also observed in healthy donor Siglec-9<sup>+</sup> CD8<sup>+</sup> T cells (Supplementary Fig. S7). A correlation between genes encoding Siglec-9, PD-1, and CD8 $\alpha$  or CD8 $\beta$  was also observed in tumors based on the TCGA melanoma dataset (Fig. 5B). The potential for functional redundancy between the Siglec-9 and PD-1 regulatory pathways was tested in the redirected cytotoxicity assay using CD8<sup>+</sup> T cells sorted from healthy donors against P815 cells, as these cells upregulate murine PD-L1 and to a lesser extent PD-L2 upon IFN $\gamma$  stimulation (Supplementary Fig. S8), both of which are known ligands of human PD-1 (36,37). In this setting, consistent with the observed co-expression pattern, Siglec-9<sup>+</sup> CD8<sup>+</sup> T cells, but not Siglec-9<sup>-</sup> cells, responded to treatment with the PD-1 checkpoint inhibitor pembrolizumab. The combined blockade resulted in synergistic effects on cytotoxicity (Fig. 5C). Deep-sequencing of the TCRV $\beta$  chains from these melanoma TILs revealed predominant clonotypes with co-occurrence in both Siglec-9<sup>+</sup> and Siglec-9<sup>-</sup> CD8<sup>+</sup> T-cell subsets (Fig. 5D), suggesting that Siglec-9 expression might be induced in the melanoma tumor microenvironment.

## DISCUSSION

In humans, as opposed to other hominids, only a minority of circulating human T cells express Siglecs (21,22), which are glycan-binding receptors (lectins) that recognize sialic acid-containing glycans (sialoglycans). The role and relevance of Siglecs in the control of T cells and the characteristics of Siglec-expressing T cells remain unexplored. We observed that the majority of tumor-infiltrating CD8<sup>+</sup> T cells in all investigated melanoma tissues expressed Siglec-9. Siglec-expressing T cells in the tumors, but also their counterparts circulating at lower numbers in the peripheral blood of both melanoma patients and healthy individuals, predominantly consisted of effector memory cells. Further analysis confirmed the previous clonal expansion of Siglec-9<sup>+</sup> CD8<sup>+</sup> T cells, which exhibited T-cell effector functionality (38,39). When stimulated using anti-CD3 and anti-CD28, Siglec-9<sup>+</sup> CD8<sup>+</sup> T cells had higher proliferation and responses compared to Siglec-9<sup>-</sup> CD8<sup>+</sup> T cells. On the other hand, engagement of the ITIM-containing Siglec-9 by anti-Siglec-9 significantly suppressed TCR-signaling and effector functions, which was associated with phosphorylation of Siglec-9 and SHP-1, but not SHP-2, in human primary CD8<sup>+</sup> T cells. These results suggest that inhibitory Siglec-9-mediated signaling pathways may prevail over antibody-mediated sequestering effects. In line with this observation, in Jurkat cells, Siglec-9 has been shown to associate preferentially with SHP-1, and not SHP-2 (21). The preference for SHP-1 might contribute to the synergistic effects of concomitant PD-1 engagement, a receptor that also contains an ITIM and preferentially recruits SHP-2 in T cells (36,40). In patients positively responding to pembrolizumab treatment, the blockade of Siglec-9 could enhance the host immune response against cancer and could represent an alternative target for patients with poor responses to pembrolizumab treatment. We observed co-expression of Siglec-9 with

several known inhibitory T-cell receptors, e.g. PD-1, CTLA-4 and Tim-3, in healthy individuals and melanoma patients, with the highest correlation being with PD-1. Despite this inhibitory phenotype, functional responses of Siglec-9<sup>+</sup> CD8<sup>+</sup> T cells to CD3/CD28 co-stimulation were higher than that observed for their Siglec-9<sup>-</sup> counterparts *in vitro*. Based on the high expression of Siglec-9 ligands on most tumor cells in primary and metastatic melanoma specimens and the co-occurrence of Siglec-9 expression on the majority of intratumoral CD8<sup>+</sup> effector memory T cells, we propose a mechanism of tumor glycosylation-dependent immune resistance.

Approved immunotherapy agents include antibodies targeting key regulatory receptors on T cells, such as CTLA-4 and PD-1, that function to block the inhibitory receptor signaling that prevents effective antitumor responses (5). However, the clinical success of therapies targeting such immune checkpoints is limited to a subset of patients, and combination therapies to improve tumor responses (41,42) often come at the cost of increased occurrence of immune-related adverse events (irAEs) (43,44). Clinical trials directed at empirically testing novel combinations has led to operational difficulties, such as competition in recruiting subjects, and the need for mechanism-based approaches to immune combinations has been recognized (1,45). Conceptually, targeting immunological checkpoints that include dominant regulatory circuits confined to the tumor microenvironment, such as Siglec-9 receptor-ligand interactions, might allow to selectively unleash the restricted repertoire of tumor-infiltrating T cells, while reducing the potential for uncontrolled T-cell activation and associated irAEs (43,44).

The reported findings support evidence for an immunosuppressive role of tumor glycosylation (21,22) by showing that tumor-intrinsic hypersialylation inhibits effector functions of Siglec-9<sup>+</sup> cytotoxic T cells, which represented the major fraction of intratumoral CD8<sup>+</sup> T cells in melanoma. The functional state of these cells

combined with signatures of clonal expansion supports the concept that co-inhibitory receptor expression on cytotoxic T cells may not be sufficient to distinguish exhaustion from activation (28). These results also suggest that Siglec-9<sup>+</sup> CD8<sup>+</sup> T cells may play a key role in adaptive immunity acquired during clonal expansion (28) and may reflect an inherent mechanism of resistance to immunotherapy. Diffuse expression of Siglec-9 ligands has also been observed in breast, lung, colon, and renal cancers, as well as leukemia (16,17), suggesting that the Siglec-9 pathway may function as a checkpoint molecule in other cancers in addition to melanoma. Targeting the tumor-restricted establishment of the functional Siglec-9 receptor-ligand axis, resulting from the co-occurrence of specific tumor glycosylation patterns and clonally restricted, tumor-confined Siglec-9<sup>+</sup> cytotoxic T cells, may provide a strategy to improve immunotherapeutic treatments for cancer.

## ACKNOWLEDGMENTS

We thank Ingrid Helsen for technical assistance. **Funding:** Research in the laboratory of S.V.G was supported by Swiss National Science Foundation (SNSF) grants 310030\_162552 and 310030\_184757, by the Swiss Cancer League/Swiss Cancer Research grants KFS-3941-08-2016 and KFS-3248-08-2013, the Novartis Foundation for medical-biological research, and Palleon Pharmaceuticals Inc., Waltham MA (USA). H.U.S. received support from the Swiss National Science Foundation (grants No. 310030-166473 and 310030\_184816) and the European Union's Horizon 2020 research and innovation program (Marie Skłodowska-Curie grant No. 642295; MEL-PLEX). C.J. received support by the SNSF (PMPDP3\_129022, Marie-Heim Vögtlin Program and PZ00P3\_161459, Ambizione Program). **Competing interests:** The authors declare no conflict of interest. **Data and materials availability:** All data is available in the manuscript or the supplementary materials.

## CONFLICT OF INTEREST

The authors declare no conflict of interest.

## REFERENCES

1. Ribas A, Wolchok JD. Cancer immunotherapy using checkpoint blockade. *Science* 2018;**359**:1350–5.
2. Couzin-Frankel J. Breakthrough of the year 2013. *Cancer Immunotherapy. Science* 2013;**342**:1432–3.
3. Chen DS, Mellman I. Elements of cancer immunity and the cancer–immune set point. *Nature* 2017;**541**:321–30.
4. Sharma P, Hu-Lieskovan S, Wargo JA, Ribas A. Primary, Adaptive, and Acquired Resistance to Cancer Immunotherapy. *Cell* 2017;**168**:707–23.
5. Sharma P, Allison JP. The future of immune checkpoint therapy. *Science* **2015**;348:56–61.
6. Sharma P, Allison JP. Immune checkpoint targeting in cancer therapy: Toward combination strategies with curative potential. *Cell* 2015;**161**:205–14.
7. Jerby-Arnon L, Shah P, Cuoco MS, Rodman C, Su M-J, Melms JC, et al. A Cancer Cell Program Promotes T Cell Exclusion and Resistance to Checkpoint Blockade. *Cell* 2018;**175**:984–997.
8. O'Donnell JS, Long G V., Scolyer RA, Teng MWL, Smyth MJ. Resistance to PD1/PDL1 checkpoint inhibition. *Cancer Treat Rev* 2017;**52**:71–81.
9. Stowell SR, Ju T, Cummings RD. Protein Glycosylation in Cancer. *Annu Rev Pathol Mech Dis* 2015;**10**:473–510.
10. Boligan KF, Mesa C, Fernandez LE, Von Gunten S. Cancer intelligence acquired (CIA): Tumor glycosylation and sialylation codes dismantling antitumor defense. *Cell Mol Life Sci.* 2015;**72**:1231–48.
11. Fuster MM, Esko JD. The sweet and sour of cancer: glycans as novel therapeutic targets. *Nat Rev Cancer* 2005;**5**:526–42.
12. Varki A. Since there are PAMPs and DAMPs, there must be SAMPs? Glycan “self-associated molecular patterns” dampen innate immunity, but pathogens can mimic them. *Glycobiology* 2011;**21**:1121–4.
13. Crocker PR, Paulson JC, Varki A. Siglecs and their roles in the immune system. *Nat Rev Immunol.* 2007;**7**:255–66.
14. Jandus C, Simon H-U, von Gunten S. Targeting Siglecs—A novel pharmacological strategy for immuno- and glycotherapy. *Biochem Pharmacol* 2011;**82**:323–32.
15. Hudak JE, Canham SM, Bertozzi CR. Glycocalyx engineering reveals a Siglec-based mechanism for NK cell immunoevasion. *Nat Chem Biol* 2014;**10**:69–75.
16. Jandus C, Boligan KF, Chijioke O, Liu H, Dahlhaus M, Démoulin T, et al. Interactions between Siglec-7 / 9 receptors and ligands influence NK cell –

dependent tumor immunosurveillance. *J Clin Invest*. 2014;**124**:1810–20.

17. Läubli H, Pearce OMT, Schwarz F, Siddiqui SS, Deng L, Stanczak MA, et al. Engagement of myelomonocytic Siglecs by tumor-associated ligands modulates the innate immune response to cancer. *Proc Natl Acad Sci* 2014;**111**:14211–6. 9
18. Beatson R, Tajadura-Ortega V, Achkova D, Picco G, Tsourouktsoglou T-D, Klausning S, et al. The mucin MUC1 modulates the tumor immunological microenvironment through engagement of the lectin Siglec-9. *Nat Immunol* 2016;**17**:1273–81.
19. Adams OJ, Stanczak MA, von Gunten S, Läubli H. Targeting sialic acid–Siglec interactions to reverse immune suppression in cancer. *Glycobiology* 2017;**28**:640–47
20. Haas Q, Simillion C, von Gunten S. A Cartography of Siglecs and Sialyltransferases in Gynecologic Malignancies: Is There a Road Towards a Sweet Future? *Front Oncol* 2018;**8**:68.
21. Ikehara Y, Ikehara SK, Paulson JC. Negative regulation of T cell receptor signaling by Siglec-7 (p70/AIRM) and Siglec-9. *J Biol Chem*. 2004;**279**:43117–25.
22. Nguyen DH, Tangvoranuntakul P, Varki A. Effects of natural human antibodies against a nonhuman sialic acid that metabolically incorporates into activated and malignant immune cells. *J Immunol* 2005;**175**:228–36.
23. Varki A. Glycan-based interactions involving vertebrate sialic-acid-recognizing proteins. *Nature* 2007;**446**:1023–9.
24. Bankhead P, Loughrey MB, Fernández JA, Dombrowski Y, McArt DG, Dunne PD, et al. QuPath: Open source software for digital pathology image analysis. *Sci Rep* 2017;**7**:16878.
25. Appay V, Douek DC, Price DA. CD8+T cell efficacy in vaccination and disease. *Nat Med*. 2008;**14**:623–8.
26. Palucka AK, Coussens LM. The Basis of Oncoimmunology. *Cell*. 2016;**164**:1233–47.
27. Geginat J, Lanzavecchia A, Sallusto F. Proliferation and differentiation potential of human CD8+ memory T-cell subsets in response to antigen or homeostatic cytokines. *Blood* 2003;**101**:4260–6.
28. Tirosh I, Izar B, Prakadan SM, Wadsworth MH, Treacy D, Trombetta JJ, et al. Dissecting the multicellular ecosystem of metastatic melanoma by single-cell RNA-seq. *Science* 2016;**352**:189–96.
29. Wherry EJ, Ha S-J, Kaech SM, Haining WN, Sarkar S, Kalia V, et al. Molecular Signature of CD8+ T Cell Exhaustion during Chronic Viral Infection. *Immunity* 2007;**27**:670–84.

30. Fuertes Marraco SA, Neubert NJ, Verdeil G, Speiser DE. Inhibitory Receptors Beyond T Cell Exhaustion. *Front Immunol* 2015;**6**:310.
31. Crocker PR, Paulson JC, Varki A. Siglecs and their roles in the immune system. *Nat Rev Immunol* 2007;**7**:255–66.
32. von Gunten S, Yousefi S, Seitz M, Jakob SM, Schaffner T, Seger R, et al. Siglec-9 transduces apoptotic and nonapoptotic death signals into neutrophils depending on the proinflammatory cytokine environment. *Blood* 2005;**106**:1423–31.
33. Macauley MS, Crocker PR, Paulson JC. Siglec-mediated regulation of immune cell function in disease. *Nat Rev Immunol* 2014;**14**:653–66.
34. Baerlocher GM, Vulto I, de Jong G, Lansdorp PM. Flow cytometry and FISH to measure the average length of telomeres (flow FISH). *Nat Protoc* 2006;**1**:2365–76.
35. Becattini S, Latorre D, Mele F, Foglierini M, De Gregorio C, Cassotta A, et al. Functional heterogeneity of human memory CD4+ T cell clones primed by pathogens or vaccines. *Science* 2015;**347**:400–6.
36. Latchman Y, Wood CR, Chernova T, Chaudhary D, Borde M, Chernova I, et al. PD-L2 is a second ligand for PD-1 and inhibits T cell activation. *Nat Immunol* 2001;**2**:261–8.
37. Freeman GJ, Long AJ, Iwai Y, Bourque K, Chernova T, Nishimura H, et al. Engagement of the PD-1 immunoinhibitory receptor by a novel B7 family member leads to negative regulation of lymphocyte activation. *J Exp Med* 2000;**192**:1027–34.
38. Haas A, Weckbecker G, Welzenbach K. Intracellular phospho-flow cytometry reveals novel insights into TCR proximal signaling events. A comparison with Western blot. *Cytom Part A* 2008;**73**:799–807.
39. Hogan SA, Courtier A, Cheng PF, Jaberg-Bentele NF, Goldinger SM, Manuel M, et al. Peripheral blood TCR repertoire profiling may facilitate patient stratification for immunotherapy against melanoma. *Cancer Immunol Res* 2018;**4**:959–67.
40. Chemnitz JM, Parry R V, Nichols KE, June CH, Riley JL. SHP-1 and SHP-2 associate with immunoreceptor tyrosine-based switch motif of programmed death 1 upon primary human T cell stimulation, but only receptor ligation prevents T cell activation. *J Immunol* 2004;**173**:945–54.
41. Sharma P, Allison JP. Immune checkpoint targeting in cancer therapy: toward combination strategies with curative potential. *Cell* 2015;**161**:205–14.
42. Schmidt C. The benefits of immunotherapy combinations. *Nature* 2017;**552**:S67–9.
43. Boutros C, Tarhini A, Routier E, Lambotte O, Ladurie FL, Carbonnel F, et al. Safety profiles of anti-CTLA-4 and anti-PD-1 antibodies alone and in

combination. *Nat Rev Clin Oncol* 2016;**13**:473–86.

44. Sanmamed MF, Chen L. A Paradigm Shift in Cancer Immunotherapy: From Enhancement to Normalization. *Cell* 2018;**175**:313–26.
45. Kaiser J. Too much of a good thing? *Science* 2018;**359**:1346–7.

## FIGURE LEGENDS

**Figure 1. Siglec-9 defines a subset of effector memory CD8<sup>+</sup> T cells that prevails in the melanoma tumor microenvironment.** (A) Representative flow cytometry plots of Siglec-9 on CD8<sup>+</sup> T cells from the peripheral blood (PB) of healthy donors (HD) or melanoma patients, and melanoma tumor-infiltrating lymphocytes (TILs) and (B) quantitative analysis of Siglec-9 on CD8<sup>+</sup> T cells from the PB of healthy donors (n=23) or melanoma patients (n=8), and melanoma TILs (n=6). (C) Pairwise scatter plot representation of RNA expression (log2) of Siglec-9 compared to CD8α and CD8β in melanoma specimens (n=469), according to TCGA Network data. (D-E) Flow cytometric, multiparametric assessment of Siglec-9 surface expression on naive, central memory (CM), effector memory (EM), and CD45RA<sup>+</sup> effector memory (EMRA) CD8<sup>+</sup> T-cell subsets in the PB of healthy donors (n=8) or melanoma patients (n=6), and melanoma TILs (n=5); (D) quantitative analysis and (E) illustration. (F) Pairwise scatter plot representation of RNA expression of Siglec-9 compared to granzyme B, perforin, IFNγ, and TNFα in melanoma specimens (n=469), according to TCGA Network data. Statistical analysis was performed by one-way ANOVA followed by followed by (B) Holm-Sidak's or (D) Bonferroni post-test. Error bars show s.d. \**P*<0.05, \*\**P*<0.01, \*\*\**P*<0.001.

**Figure 2. Tumor expression of Siglec-9 ligands inhibits TCR signaling and effector functions of Siglec-9<sup>+</sup> CD8<sup>+</sup> T cells.** (A,B) Immunohistochemical tissue microarray analysis (TMA) for Siglec-9 ligand expression in intradermal nevi (IDN; n=7), primary melanoma (n=62), and metastatic melanoma (n=20). Representative examples co-stained with melanoma marker (A) melan-A and DAPI and (B) quantitative analysis (int. D/A: integrated density/tumor area) using box-and-whisker diagrams (median, lower and upper quartiles; horizontal lines define minimum and

maximum). (C) Immunohistochemical TMA analysis for Siglec-9 ligand<sup>+</sup> cancer cells in melanoma (n=37) and metastatic melanoma (n=30). Data are present median and interquartile range. (D) RNA expression of sialyltransferases in melanoma (n=469), based on TCGA Network data computed by a dendrogram clustering algorithm. Cliques' numbers are arbitrary given from left to right for expression pattern rising from low to high RNA signal. (E) Confocal immunofluorescence microscopy analysis indicating localization of Siglec-9 ligands on the surface of P815 cells with and without neuraminidase treatment (25 mU) (sialic acid dependency). (F-K) Target cell neuraminidase treatment effects on responses of redirected CD8<sup>+</sup> T cell from healthy donors upon coculture with anti-CD3–loaded P815 tumor cells for (F) 4 or (G-I) 5 hours. (F) Cytotoxicity, (G) CD107a mobilization, and (H) intracellular IFN $\gamma$  or (I) TNF $\alpha$  production. (J, K) Flow cytometric monitoring of the phosphorylation status of intracellular TCR signaling molecules (J) pZAP-70 and (K) pSLP-76 upon exposure of T cells to anti-CD3–loaded P815 tumor cells for 10 minutes. Relative phosphorylation changes as a consequence of neuraminidase treatment (desialylation) are shown. (F-K) Effector/target (E/T) ratio at 3:1. Statistical analysis was performed by one-way ANOVA followed by followed by (B) Holm-Sidak's or (F-H) Bonferroni post-test or (I-K) Student's *t*-test. \**P*<0.05, \*\**P*<0.01, \*\*\**P*<0.001; n.s., not significant. Error bars show s.d. Data are representative of at least (K) 3, (J) 5, or (F-H) 6 experiments.

**Figure 3. Inhibition of TCR signaling and CD8<sup>+</sup> T-cell effector functions by Siglec-9<sup>+</sup> is associated with phosphorylation of SHP-1 but not SHP-2.** (A) Redirected cytotoxicity assay using healthy donor CD8<sup>+</sup> T cells against anti-CD3–loaded P815 tumor cells (3:1 E/T ratio) upon engagement by agonistic anti–Siglec-9 or mouse IgG1 as isotype control (3  $\mu$ g/mL). (B,C) Intracellular cytokine production of

(B) IFN $\gamma$  or (C) TNF $\alpha$  by healthy donor CD8<sup>+</sup> T cells upon engagement by agonistic anti-Siglec-9 (3  $\mu$ g/mL) following 5 hours culture with anti-CD3 and anti-CD28 co-stimulation (both 1  $\mu$ g/mL). (D-E) Flow cytometric monitoring of the phosphorylation status of intracellular TCR signaling molecules (D) pZAP-70 and (E) pSLP-76 upon healthy donor CD8<sup>+</sup> T cell engagement by agonistic anti-Siglec-9 with co-stimulation by anti-CD3 and anti-CD28 (both 1  $\mu$ g/mL). (F) Phosphorylation status of Siglec-9 CD8<sup>+</sup> T cells from healthy donors treated with anti-Siglec-9 or isotype control (both 3  $\mu$ g/mL) for 1 or 5, 10, and 15 minutes compared to time-matched controls (ratio) measured by ELISA. (G) Densitometric analysis of immunoblots demonstrating SHP-1 or SHP-2 phosphorylation in CD8<sup>+</sup> T cells from healthy donors treated with anti-Siglec-9 or isotype control (both 3  $\mu$ g/mL) for 1 or 5, 10, and 20 minutes compared to time-matched controls (ratio). (H) Pairwise scatter plot representation of RNA expression (log2) of Siglec-9 compared to SHP-1 and SHP-2 in melanoma specimens (n=469), according to TCGA Network data. Statistical analysis was performed by Student *t*-test (A-E). \**P*<0.05, \*\**P*<0.01. Data are representative of at least (D) three, (A-C,E,G) four experiments.

**Figure 4. Siglec-9<sup>+</sup> CD8<sup>+</sup> T-cell clonotypes, chemokine receptor expression, and function upon TCR stimulation *in vitro*.** Analysis of peripheral blood CD8<sup>+</sup> T cell from healthy donors. (A) Representative flow cytometry plots and (B) flow cytometric quantitative analysis demonstrating intracellular IFN $\gamma$  or TNF $\alpha$  production in CD8<sup>+</sup> T-cell subsets following 5 hours culture with co-stimulation by anti-CD3 and anti-CD28 (1  $\mu$ g/mL). (C) Representative flow cytometric data illustrating proliferation of anti-CD3 and anti-CD28 (1 $\mu$ g/mL) co-stimulated CD8<sup>+</sup> T-cell subsets, assessed four days post-activation (D) Telomere length analysis of CD8<sup>+</sup> T-cell subsets from healthy donors The box shows 25th to 75th percentile with median, error bars mark 1st to

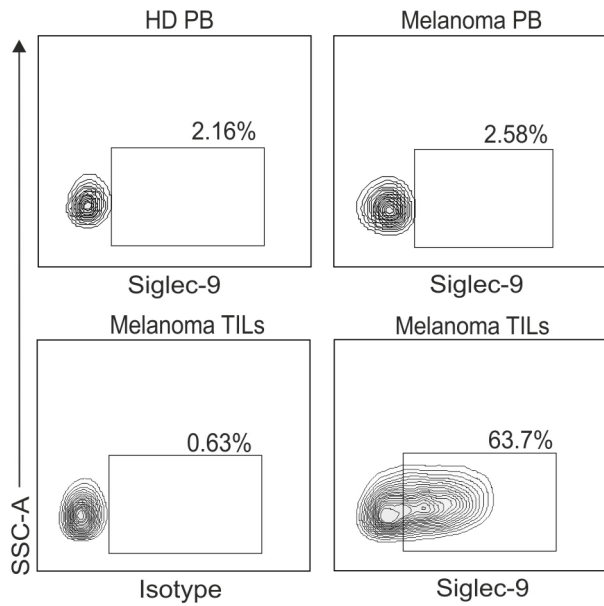
99th percentile. (E) Flow cytometric analysis of chemokine receptors on the surface of CD8<sup>+</sup> T-cell subsets. (F) Frequency distribution of clonotypes based on the 10 most prevalent nucleotide TCRv $\beta$  chains within CD8<sup>+</sup> T-cell subsets of healthy donors. (G) Nucleotide chain distribution of clonotype frequency in Siglec-9<sup>+</sup> CD8<sup>+</sup> T cells (x-axis) and Siglec-9<sup>-</sup> CD8<sup>+</sup> T cells (y-axis) from donor TS-02. Orange and blue dots represent clonotypes that were statistically found more frequently in one of these two populations based on Fisher's exact test and are above the threshold for statistical comparison (red dotted line, indicating minimum cumulative number of templates). The black dotted line indicates frequency equality. (H) Illustration of the 10 most expanded TCRv $\beta$  nucleotide chain distribution frequency in CD8<sup>+</sup> T-cell subsets isolated from donor TS-02. \* $P$ <0.05, \*\* $P$ <0.01, \*\*\* $P$ <0.001, Student's  $t$ -test. Data are representative of at least (E) three, (H) five, or (G) six experiments.

**Figure 5. Co-inhibitory receptor expression and clonotype analysis of tumor-infiltrating Siglec-9<sup>+</sup> CD8<sup>+</sup> T cells in melanoma.** (A) Radar chart of flow cytometric data demonstrating surface co-expression of Siglec-9 with PD-1, CTLA-4, BTLA, LAG3, or Tim-3 on CD8<sup>+</sup> T cells from melanoma tumor-infiltrating lymphocytes (TILs;  $n$ =4). Black line represents the mean, grey lines the SD. (B) Scatter diagram representation of RNA expression (log2) of Siglec-9, PD-1, and CD8 $\alpha$  or CD8 $\beta$  in melanoma specimens ( $n$ =469). Data are obtained from TCGA. (C) Redirected cytotoxicity of healthy donor CD8<sup>+</sup> T cells against anti-CD3-loaded P815 tumor cells (3:1 E/T ratio) for 4 hours upon anti-PD-1 (10  $\mu$ g/mL; pembrolizumab), target cell neuraminidase treatment (2.5 mU), or both. Plot represents median with 5-95 percentile whiskers. (D) TCRv $\beta$  nucleotide chain distribution frequency in CD8<sup>+</sup> T-cell subsets isolated from the TILs of melanoma patient ( $n$ =1). Statistical analysis was

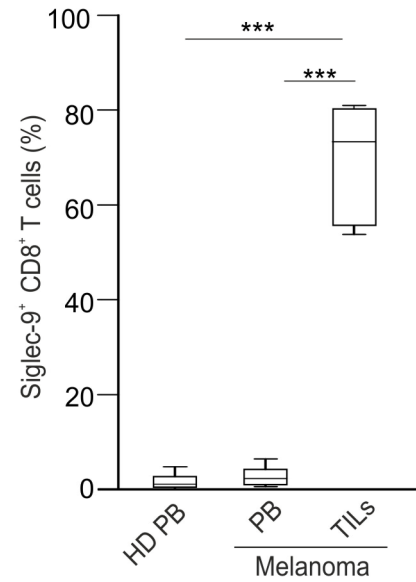
performed by one-way ANOVA followed by (C) Bonferroni post-test. \*\* $P < 0.01$ ; n.s., not significant. Data are representative of at least (A) four or (C) 9 experiments.

**Figure 1**

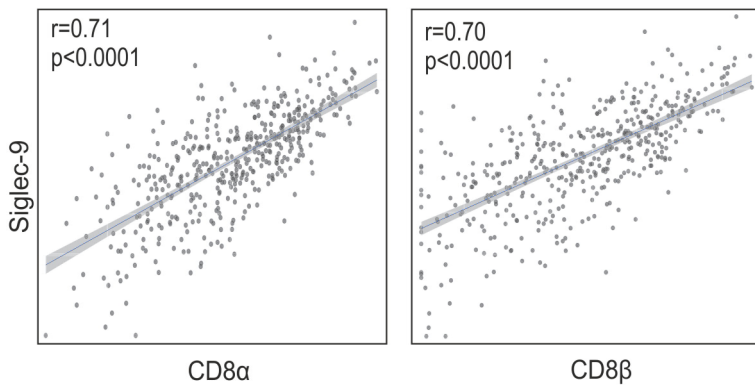
**A**



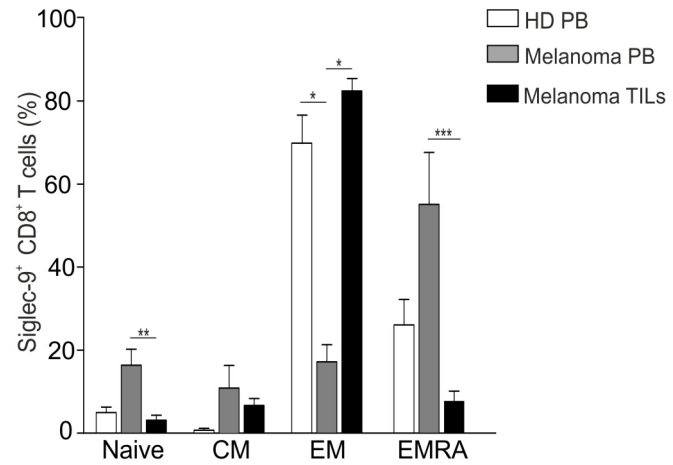
**B**



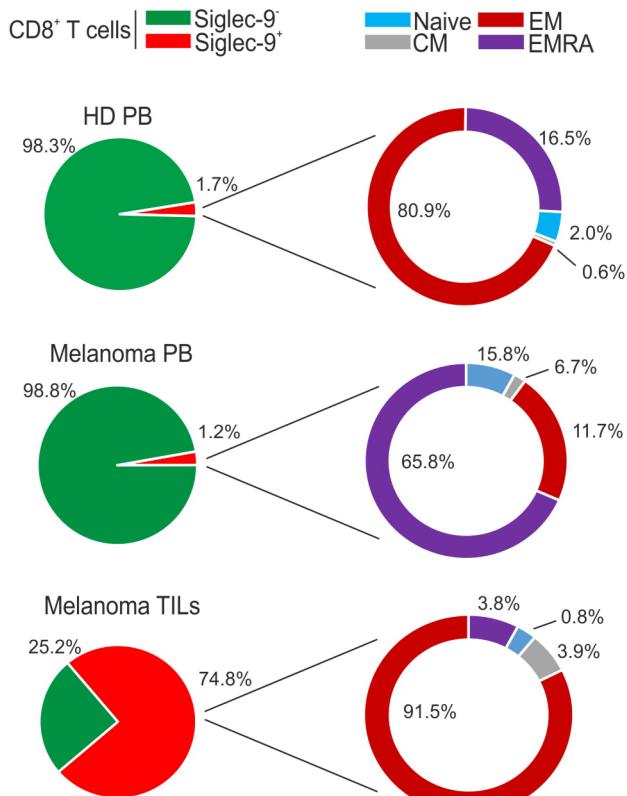
**C**



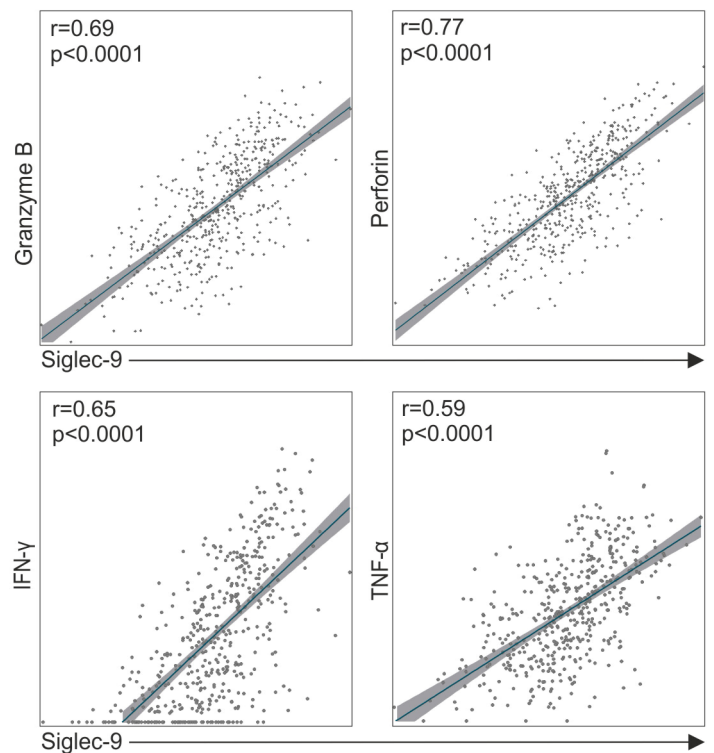
**D**



**E**



**F**



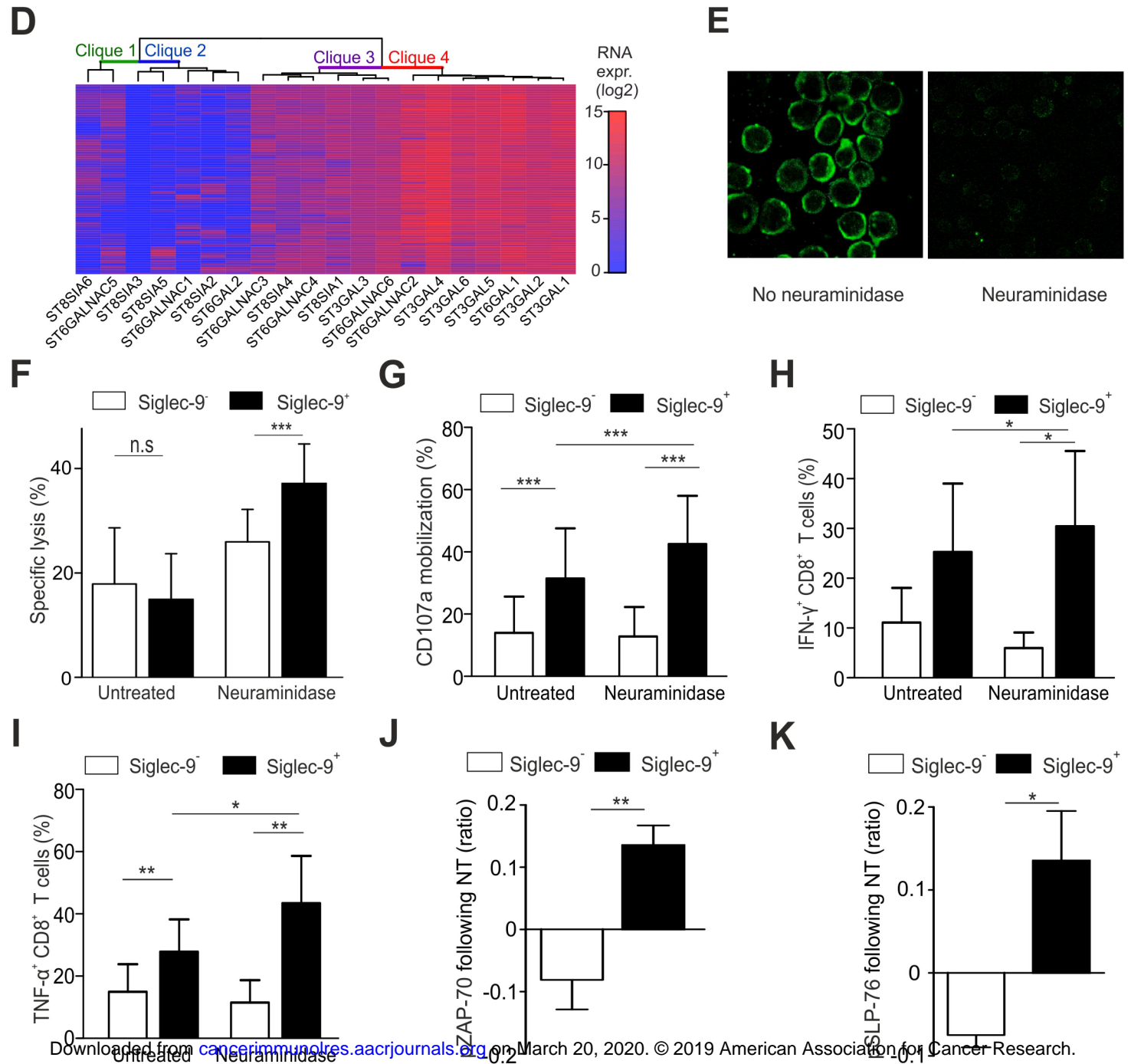
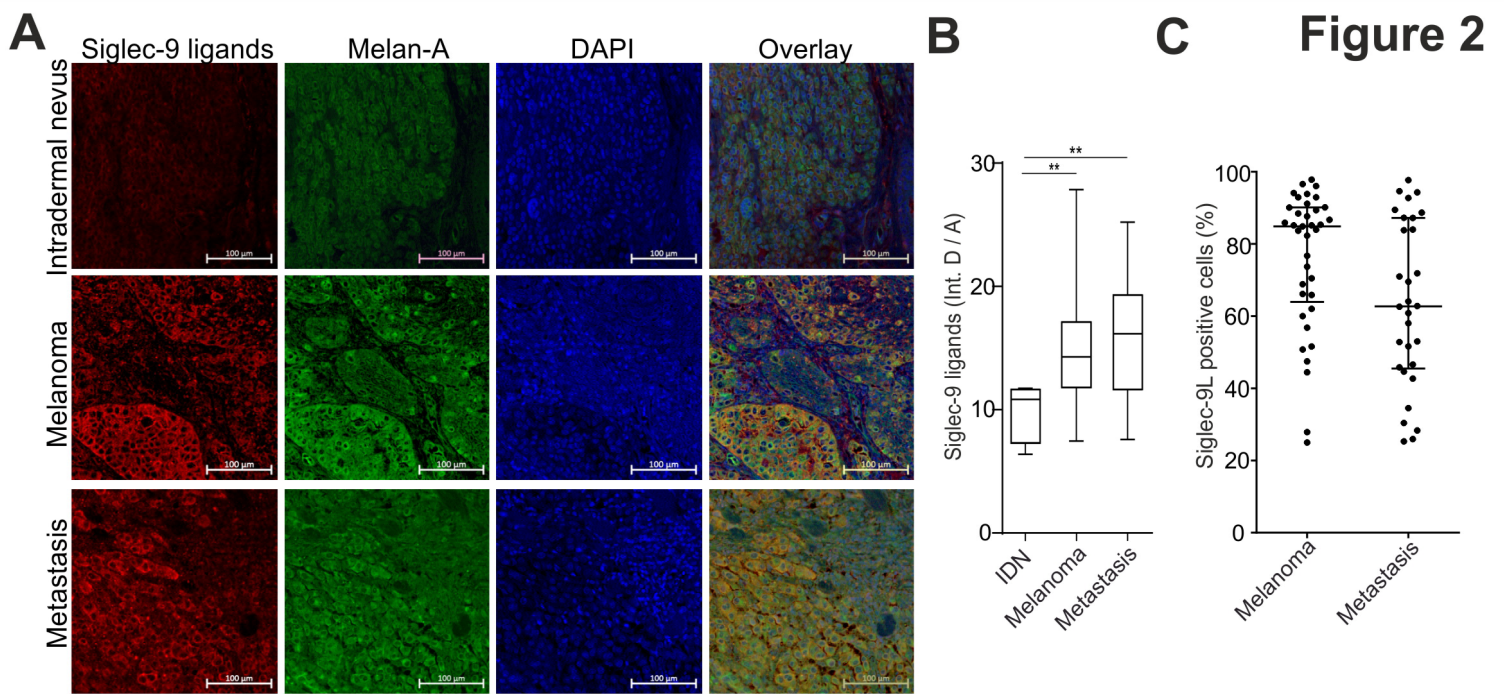
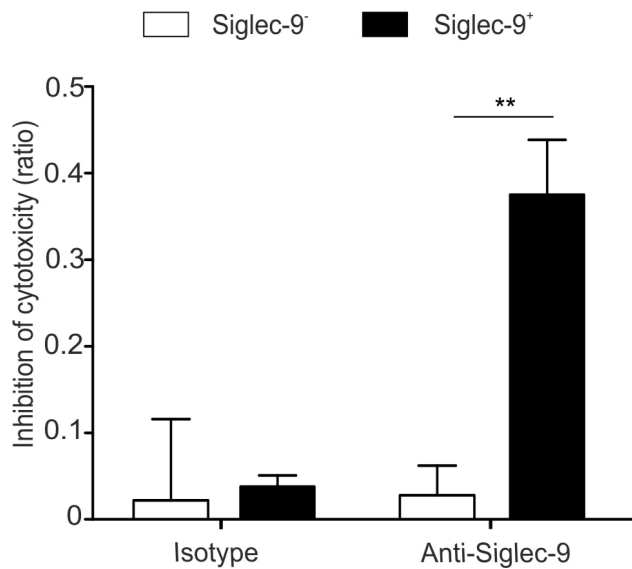
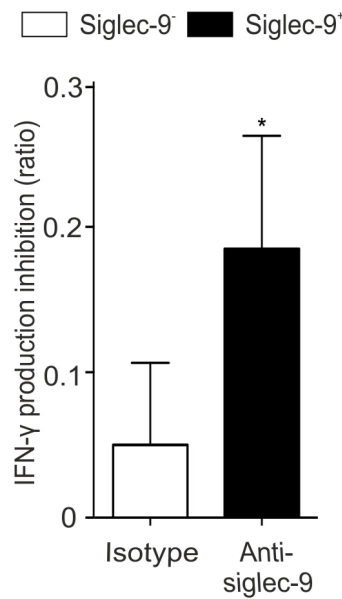


**Figure 3**

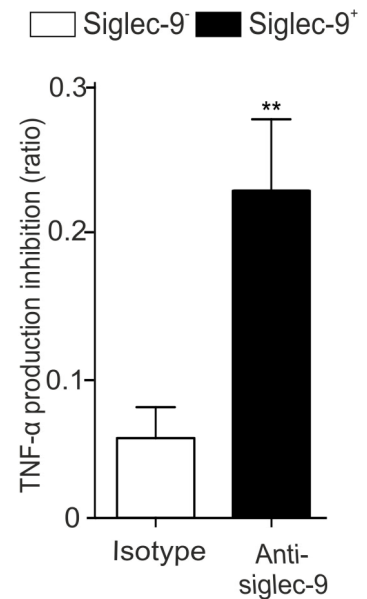
**A**



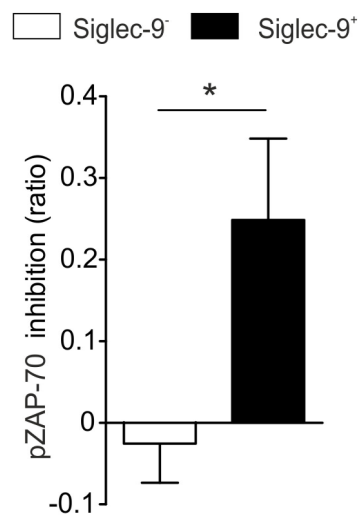
**B**



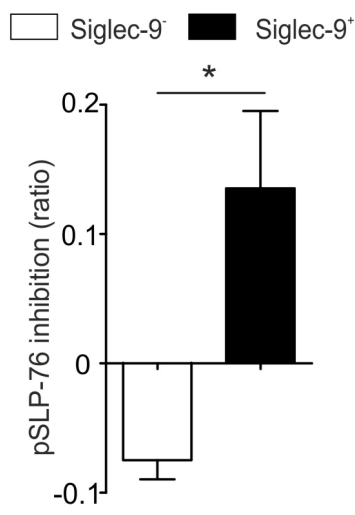
**C**



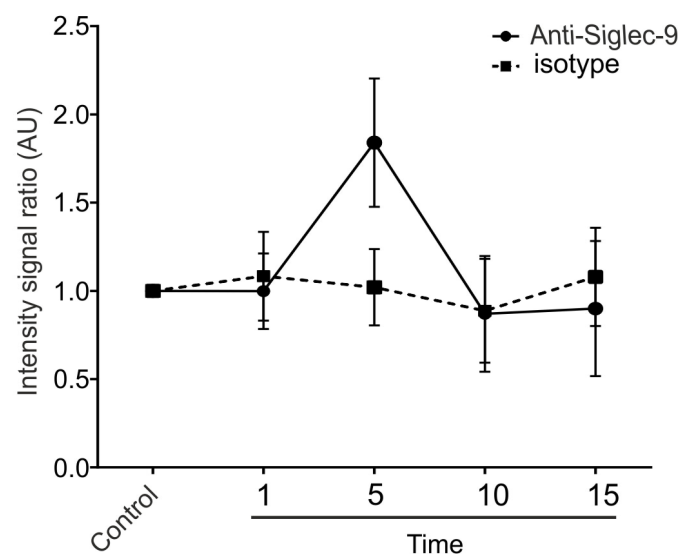
**D**



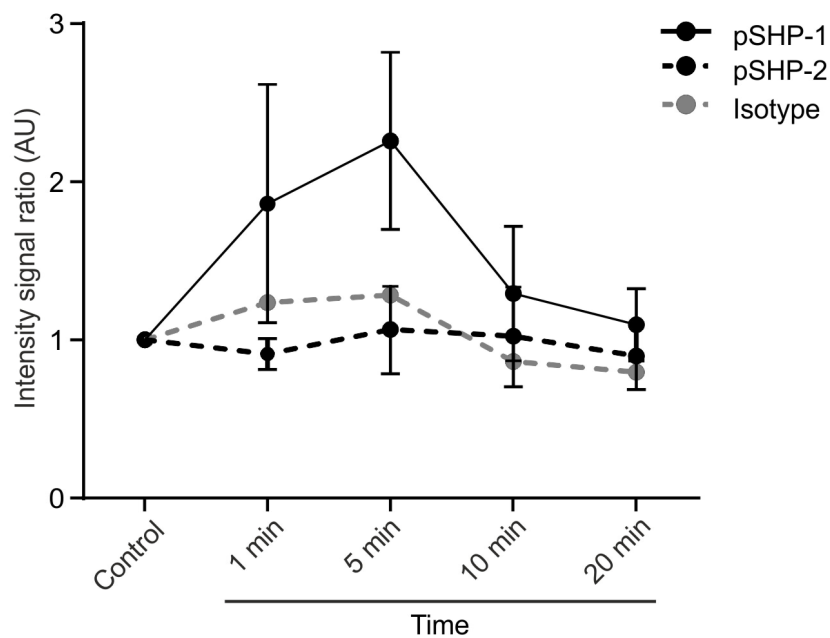
**E**



**F**



**G**



**H**

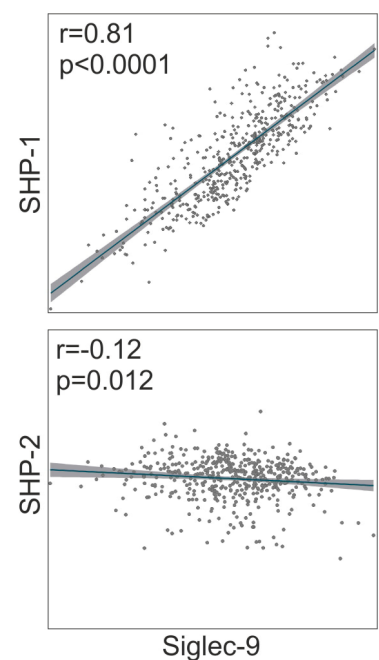


**Figure 4**

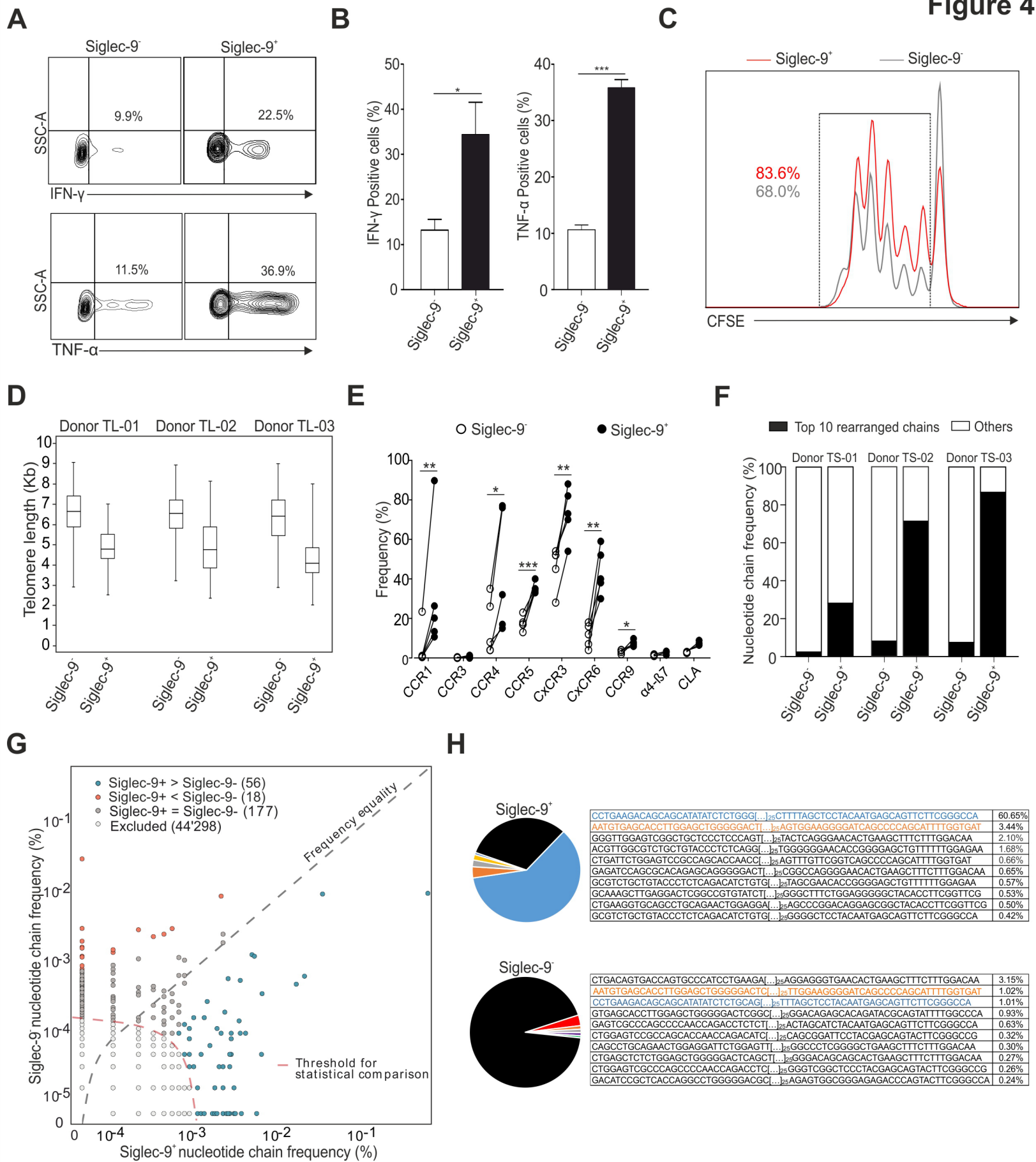
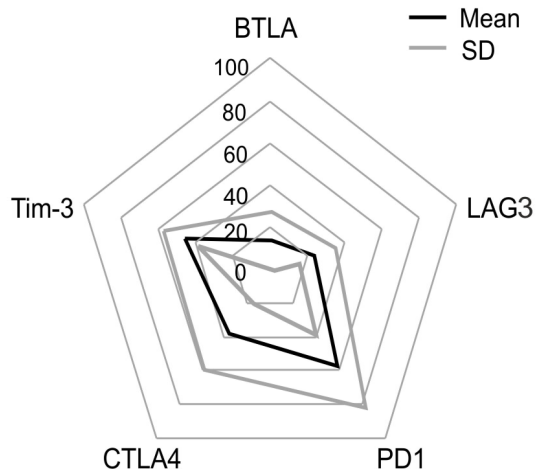
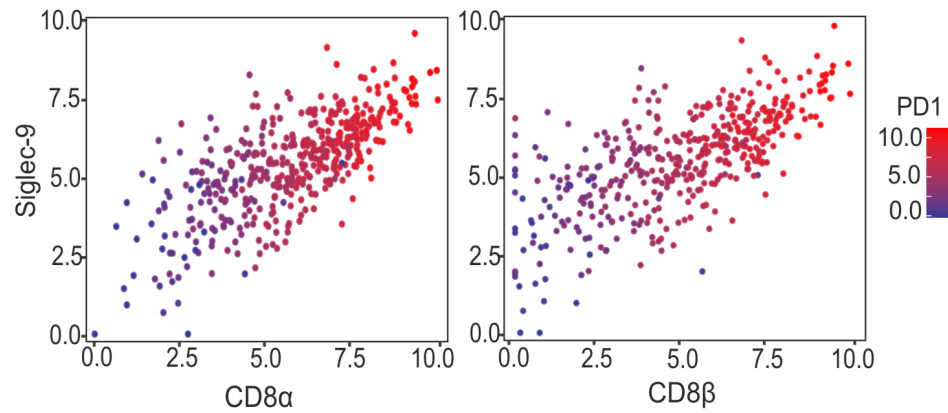


Figure 5

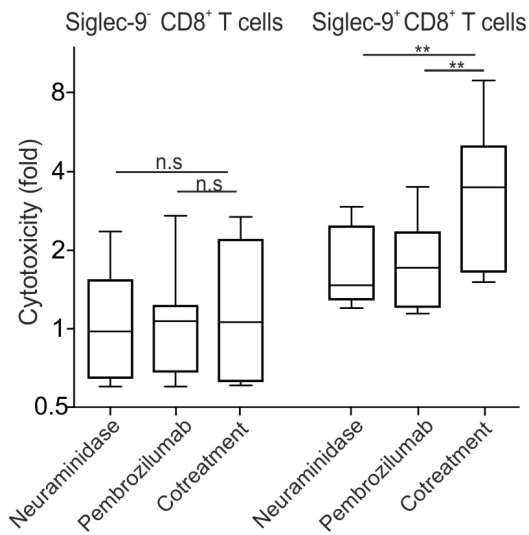
A



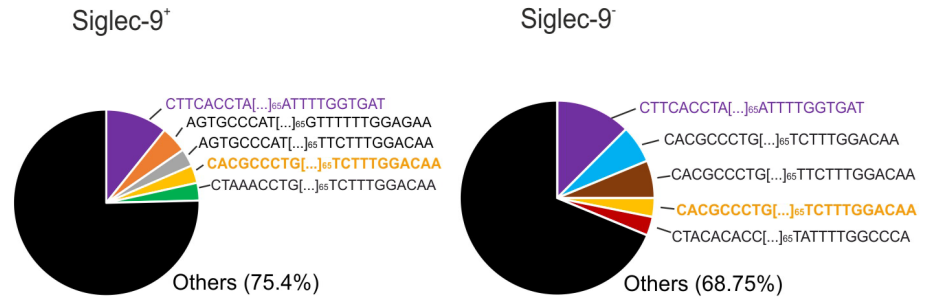
B



C



D



# Cancer Immunology Research

## Siglec-9 regulates an effector memory CD8<sup>+</sup> T-cell subset that congregates in the melanoma tumor microenvironment

Quentin Haas, Kayluz Frias Boligan, Camilla Jandus, et al.

*Cancer Immunol Res* Published OnlineFirst April 15, 2019.

<b>Updated version</b>	Access the most recent version of this article at: doi: <a href="https://doi.org/10.1158/2326-6066.CIR-18-0505">10.1158/2326-6066.CIR-18-0505</a>
<b>Supplementary Material</b>	Access the most recent supplemental material at: <a href="http://cancerimmunolres.aacrjournals.org/content/suppl/2019/04/13/2326-6066.CIR-18-0505.DC1">http://cancerimmunolres.aacrjournals.org/content/suppl/2019/04/13/2326-6066.CIR-18-0505.DC1</a>
<b>Author Manuscript</b>	Author manuscripts have been peer reviewed and accepted for publication but have not yet been edited.

<b>E-mail alerts</b>	<a href="#">Sign up to receive free email-alerts</a> related to this article or journal.
<b>Reprints and Subscriptions</b>	To order reprints of this article or to subscribe to the journal, contact the AACR Publications Department at <a href="mailto:pubs@aacr.org">pubs@aacr.org</a> .
<b>Permissions</b>	To request permission to re-use all or part of this article, use this link <a href="http://cancerimmunolres.aacrjournals.org/content/early/2019/04/13/2326-6066.CIR-18-0505">http://cancerimmunolres.aacrjournals.org/content/early/2019/04/13/2326-6066.CIR-18-0505</a> . Click on "Request Permissions" which will take you to the Copyright Clearance Center's (CCC) Rightslink site.